A non-isothermal fatigue crack growth law for the A356-T7 aluminium alloy

Elias Merhy, Luc Rémy, Habibou Maitournam, Louis Augustins

A NON-ISOTHERMAL FATIGUE CRACK GROWTH LAW FOR THE A356-T7 ALUMINUM ALLOY

E. Merhy [1,2,3*], L. Rémy[1], H. Maitournam[2] and L. Augustins[3]

[1]Centre des Matériaux, Mines Paris – ParisTech, UMR CNRS 7633, BP87 F-91003 Evry, France
[2]Laboratoire de Mécanique des Solides, CNRS URA 317, Ecole Polytechnique, 91128 Palaiseau Cedex, France
[3]PSA Peugeot Citroën, Route de Gisy, 78943 Vélizy-Villacoublay Cedex, France
*elias.merhy@hotmail.com ; elias.merhy@mpsa.com

keywords: Thermal-mechanical fatigue, Crack growth rate, Damage tolerant design, Life time prediction, A356 cast alloy

ABSTRACT

Fatigue crack growth period in cylinder heads of A356-T7 casting alloy has been found to constitute an important part of the structure's total life. Therefore, the fatigue model design should consider crack propagation life. Then, in order to find a new crack growth law, finite element simulations on a cylinder head 3D model and fatigue crack tests have been conducted as to establish the contribution of each loading parameter in governing the crack propagation.
SEM, optical microscopy and other metallographic techniques have been used to examine fracture surfaces and to analyze particles cracking. It has been found that the crack growth mechanism changes gradually at the microstructural scale with the increasing of K_{max} value. Performing tests at variable frequencies has shown important crack growth time dependence. Negative load ratio tests have revealed a primordial importance of the compressive load part on the crack advance.
Using experimental and numerical results, a new "damage tolerant" model design based on a non-isothermal crack growth prediction law has been introduced. The law is based on a corrected linear elastic fracture mechanics stress intensity factor K_p accounting for the cumulative crack tip plasticity. The law figures all of the purely fatigue effect, the crack growth under monotonic loading condition (time dependent parameter) and the effect of the compressive load on the global crack advance.

1 – INTRODUCTION

Today's higher demands regarding lower overall engines' weight yield the increasingly rely on high performance aluminum cylinder heads. PSA Peugeot Citroen cylinder heads ("HDI" diesel common rail injection engine) of A356-T7 casting alloy are actually designed using the "safe life" approach (S-N curve) based on the mechanical energy dissipated in the material.
Since even high quality cast aluminum components contain porosity, oxides and other inclusions, crack initiation life can be a small fraction of the total life. In our structure, it was found that the life spent to initiate a fatigue crack is less than the half of its total life. Therefore, the fatigue process selection should consider fatigue crack growth life.
Then, in order to find a new crack propagation law under complex multi-axial thermo-mechanical transient loading the first step was to perform finite element simulation on a cylinder head 3D model to first verify the localization of the structure's critical zone at the nose bridge between the inlet and the exhaust valve and second to determine the stress and temperature fields variation with time in that zone. As a second step, long crack fatigue tests were conducted on CT16 and SEN specimens at different load ratios, temperatures, frequencies and stress intensity factor values in order to determine the influence of each loading parameter in controlling the fatigue crack propagation. Using tests and simulation results, a new non-isothermal crack growth law is proposed.

2 – FINITE ELEMENT SIMULATION OF THE STRUCTURE

ABAQUS finite element simulation has been carried out on a cylinder head 3D model consisting of almost 340 000 ten-node tetrahedral element (C3D10) and using a unified elasto-visco-plastic constitutive model with non-linear kinematic hardening.
Numerical calculations of the cumulative viscoplastic deformation and the total dissipated energy conducted on the lower part of the cylinder head (flame deck) have shown that these parameters are essentially concentrated at the inlet/exhaust nose bridges verifying then the localization of the cylinder head's critical zone observed experimentally at these zones.
Cyclic temperature calculation on all over one nose bridge reveals a temperature gradient going, at the highest temperature of each cycle, from 230℃ at the nose bridge's lowest part (in contact with the flames) to 170℃ at its highes t part (in contact with cooling liquid).
The nose bridge's cyclic stress-strain fields simulation results have uncovered a negative stress ratio ($R \approx -0,57$) going from traction at low temperature to compression at high temperature. It has revealed also material thermal-mechanical behavior difference between the nose bridge's lower part presenting important cyclic viscoplastic response and a tendency to a plastic shakedown after almost 13 cycles and its highest part characterized by an elastic behavior manifested by a rapid elastic shakedown.
It is important to underline that our new crack growth law will be applied restrictively on the confined plasticity nose bridge part, second part relatively to the crack propagation direction. Therefore the initial crack length is sufficiently high to be limited in our work to the long cracks problem framework.

3 – EXPERIMENTAL CHARACTERIZATION OF CRACK GROWTH

A series of fatigue long crack growth tests have been conducted on two types of specimens, compact tension (CT16) for positive load ratio ($R>0$) tests and single edge notch (SEN) for $R<0$ tests, at different stress intensity factor ranges, temperatures and frequencies.

3.1 – Isothermal fatigue crack growth tests at R>0: Results and discussion

The da/dN-ΔK curves of the isothermal tests conducted at $R>0$, increasing ΔK and constant frequency are represented in figure 1. It shows that at a high frequency range (~20Hz) a

temperature increase from 20℃ to 150℃ provokes a minor raise of the crack growth rate by saving the same curve slope. Though, the load ratio augmentation from 0.1 to 0.7 causes not only an important decrease of the crack propagation threshold (ΔK_{th}) manifested by a left curve shift, but also a curve's slope augmentation. The slope accession reveals the fact that at higher K_{max} values than that experienced at R=0.1 the linear elastic fracture mechanics assumption is not suitable anymore whereas at these circumstances the crack tip plasticity cannot be neglected anymore. In addition, at such high load ratio value (R=0.7) the mean stress intensity factor is high enough to cause a crack growth under static loading.

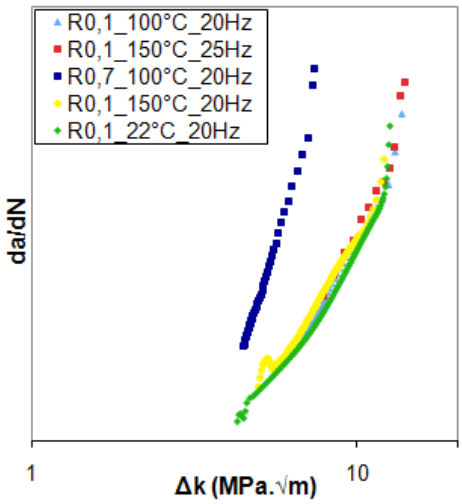

Figure 1 – Crack growth rates obtained by the increasing ΔK tests conducted on the CT16 specimens at different load ratios, temperatures and frequencies.

SEM observations of the R=0.7 test crack surface reveal a mixed mechanism crack growth, as shown in figure 2. Indeed, at low ΔK values (fig. 2.a) the image shows at the same time some fatigue traces and some ductile fracture features manifested by microvoids and dimples. However at a higher ΔK value (fig. 2.b) the crack surface shows only microvoids and dimples illustrating then, that the more K_{max} is high the more the monotonic crack advance is pronounced. A similar observation has been done on the test performed at R=0.1/100℃/20Hz that has shown an identical but more progressive mixed mechanism crack growth that goes from a total fatigue crack advance at low ΔK (beginning Paris regime) through a mixed fatigue/static load crack growth, to a total crack progression under static load at the end of the Paris regime.

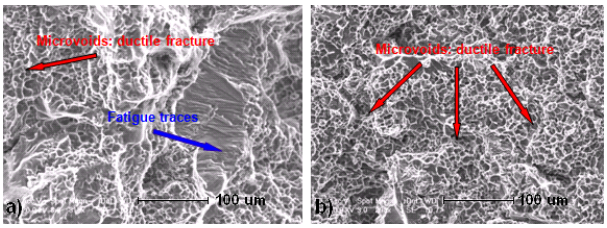

Figure 2 – Fracture faces taken in the Paris regime (regime II) of the crack growth for the test conducted at R=0.7/100℃/20Hz; a) at ΔK ≈ 5 Mpa√m ; b) at ΔK ≈ 7 Mpa√m.

For further understanding of the crack mechanisms and their controlling parameters, crack trajectory observations have been performed for several test conditions and at different crack lengths corresponding to different ΔK values. Figures 3.a and 3.c taken at the same ΔK value but at different scales show that, at low ΔK, the crack path is almost plane where crack progresses straightly in the α-Al matrix essentially with some occasionally paths through Si particles zones encountered in its way. Yet at high values of ΔK (fig. 3.b and 3.d) the crack makes a very tortuous trajectory where it shows more and more tendency to follow the Si

inter-dendrite regions. These final annotations are in perfect console with the fractography showing an increasing number of Si particles (corresponding to the observed microvoids) in crack surface with the $\Delta K/K_{max}$ augmentation. This crack path evolution phenomenon has been also reported by several authors [1-4]

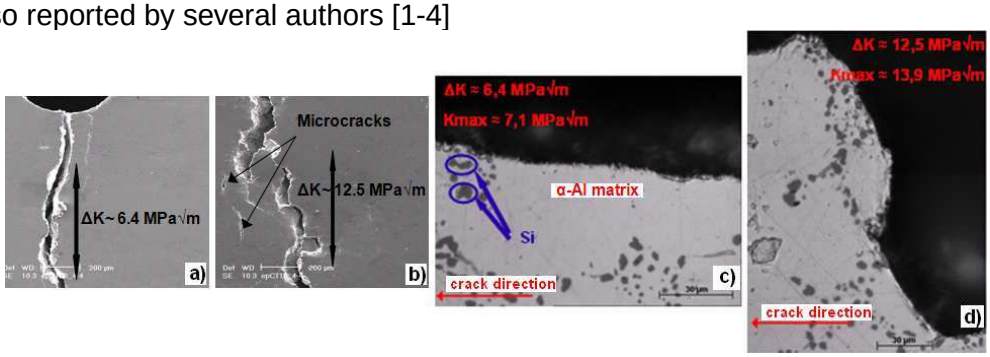

Figure 3 – Crack path for the R=0.1/100℃/20Hz test condition; a)&c) ΔK~6.4Mpa√m; b)&d) ΔK~12.5Mpa√m.

The crack mechanism and crack path changing can be explained by the amount of material damage at the crack tip region obtained at each value of K_{max} that can be described by the crack tip plasticity. Thus, when the crack tip plastic zone size is less than the range of the microstructural characteristic parameter which is the SDAS~80µm (low K_{max} value), the plastic strain energy is not relevant enough to generate damage in the inter-dendrite zone, then the crack advances in a straight plane perpendicular to the normal constraint direction. However, when the plastic zone size becomes larger than the SDAS (high K_{max} value) the plastic strain energy becomes sufficient to cause Si particle/α-Al matrix interface decohesion or even Si particles cracking. In this case, the crack leaves the perpendicular plan to the normal constraint and follows the damaged Si zones, drawing then a tortuous but more energetically favorable path.

Since it has been shown that static load could cause crack advance, numerous variable frequency fatigue crack growth tests have been carried out. Few of these tests are presented in figures 4.a and 4.b that show a clear time dependent crack growth behavior, since the frequency decrease causes drastic crack growth rate increase (without da/dN-ΔK curve slope changing for R=0.1). It is worth emphasizing that when crossing from R=0.1/ΔK=12/ K_{max}=13.3 to R=0.7/ΔK=5.5/K_{max}=18.3 curves at low frequency and high temperature show an increasing crack growth rate while curves at high frequency show decreasing cracking rate.

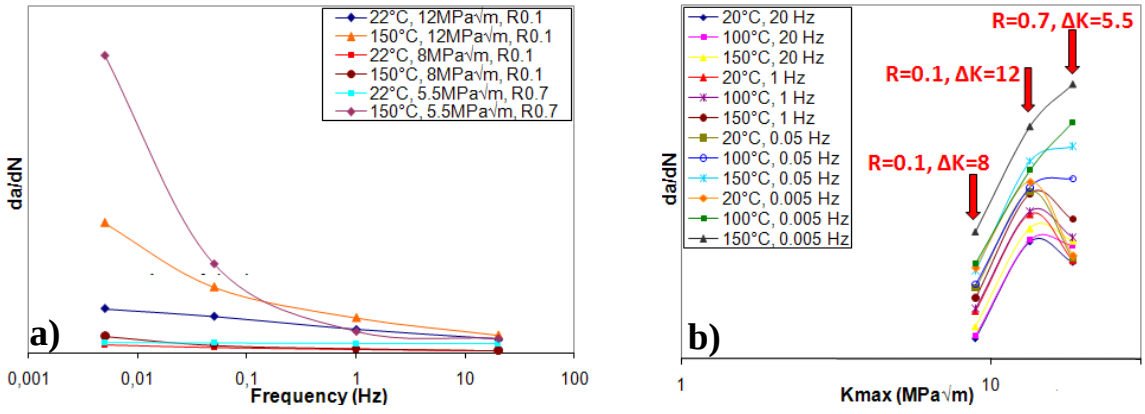

Figure 4 – Variable frequency tests performed on the CT16 specimens at different temperatures, positive load ratios and ΔK; a) da/dN-f curves; b) da/dN-ΔK curves.

This indicates that at high frequency the parameter influencing more the crack propagation rate is ΔK with a non-neglected effect of K_{max}. While at low frequency, K_{max} and T compose together the controlling parameters of the crack growth. These parameters are coupled between them in the sense that the value of one of the parameters affects the other's influence on the crack growth.

3.2 – Fatigue crack growth tests at R<0: Results and discussion

Several compliance measurements have been performed on some SEN tests at different thermal-mechanical loading and crack lengths conditions. In another hand, crack opening displacements at different distances from the crack tip have been calculated using a 3D finite element SEN model for the same measurement loading conditions. Comparing measurements and simulations results have led to the conclusion that all of temperature, frequency, stress intensity factor, and crack length have no pronounced effect on the crack opening behavior. Though, some measured K_{op} values are much below the calculated ones for the same loading conditions. Hence, at negative load ratios some microstructural phenomena are occurring in the real structure and causing further crack tip opening that cannot be spotted by the finite element simulation.
Measurements of Fracture surface roughness have unveiled its non-influence on the crack opening and consequently on the crack growth rate. Since, a load ratio decrease from R = 0.1 to R = -1 corresponds to a roughness increase and a K_{op} decrease which is in accordance with Silva's work [5].
With the aim of characterizing the compressive load contribution on the crack growth, several isothermal variable frequency fatigue crack growth tests have been carried out at different negative load ratios. All tests having the same K_{max} value, including the test at R=0.1, are sorted in a same graphic, as shown in figure 5.

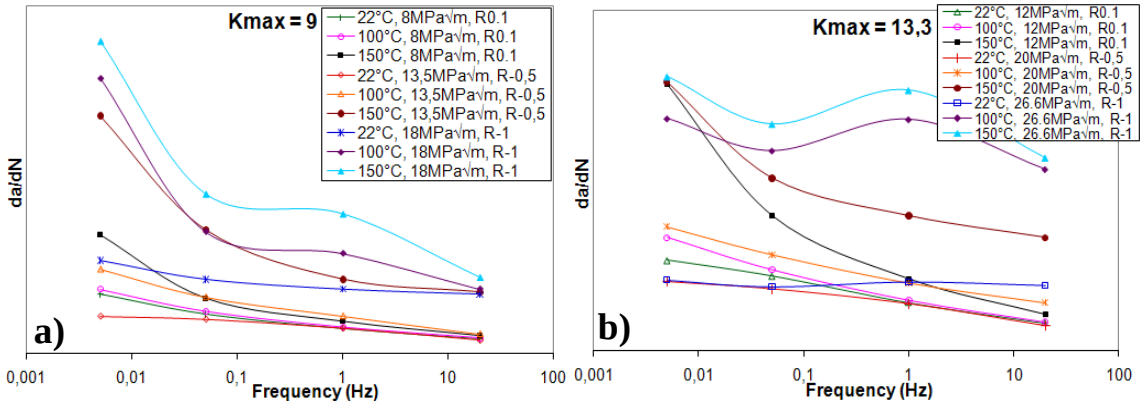

Figure 5 – Crack growth rate variation according to the frequency for the variable frequency tests performed on the SEN specimens at different temperatures, negative load ratios and ΔK.

Figure 5.a reveals that for K_{max} = 9 MPa√m all negative load ratio tests show a similar shape to that of positive load ratios and a load ratio diminution from 0.1 through -0.5 to -1, in other words the compressive load contribution, causes at several temperatures a crack growth rate raise that at its turn increases with the frequency decrease. Despite, the tests conducted at K_{max} = 13.3 MPa√m (fig. 5.b) and R = -1 show a totally different behavior since the crack growth rate have no more a parabolic accession with the frequency reduction. Moreover, the load ratio drop from 0.1 to -1 (negative load role) provokes also at K_{max} = 13.3 a crack propagation rate augmentation that, notwithstanding with the K_{max} = 9 results, decreases with the frequency diminution. Therefore, the K_{max} increase seems to have a major effect on the "negative load" crack growth decrease with the frequency reduction.
This complex behavior at negative loads can be explained as follows: knowing that Si particles are much harder than the α-Al matrix, particles and matrix deformations at their

interfaces under compression will not have the same form, as shown in the schematic of figure 6.a. The ensuring of the interface compatibility requires the multiplication of the existent geometrically necessary dislocations activating then additional slip systems in the matrix. Where, negative plastic deformation zones ($\varepsilon_p < 0$) surrounding the particles will be developed at compressive remote loads. What results finally in residual local tension stress fields ($\sigma_{res} > 0$) in the inter-dendrite eutectic zones at the crack tip area leading to the acceleration of the crack. Such phenomenon has been reported by several authors that have shown that even from fully compressive loadings, cracks can nucleate and grow till a certain crack length [6, 7]. Then at elevated K_{max}, particles, debonded and fractured by the high plastic strain energy during cycle's positive part, will not induce anymore at the negative part any residual tension stress. K_{min} diminution or the temperature increase will cause, in this case, more residual stress relaxation under an opposite remote loading than formation of new local plasticity and residual tension stress fields. For that reason the "negative load" crack growth at low frequency and high K_{max} and T becomes null.

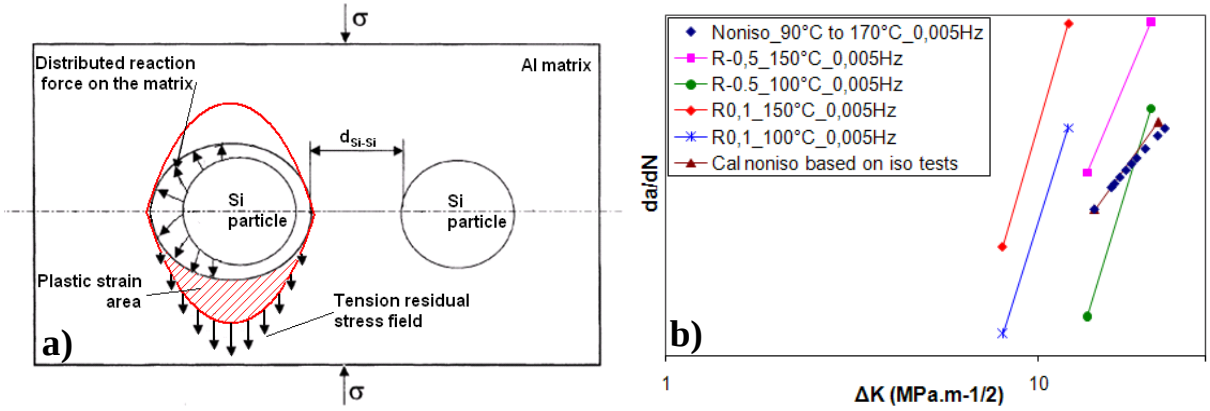

Figure 6 – a) A schematic showing the matrix/particle interface deformation, the engendered plastic strain area and the induced tension residual stress field, under remote compression load;
b) da/dN-ΔK curves of the non-isothermal test conducted on SEN specimen at R ≈ -0.5, f = 0.005Hz, σ_{max}= 112 MPa, σ_{min}=-64Mpa, T_{min}(at σ_{max})=90℃, T_{max} (at σ_{min})=170℃

An out of phase non-isothermal test has been conducted on a SEN specimen at the same thermal-mechanical real loading conditions (R ≈ -0.5, f = 0.005Hz, T_{min}(at σ_{max})=90℃, T_{max} (at σ_{min})=170℃). Figure 6.b presents the non-isothermal da /dN-ΔK curve in addition to those of the isothermal R=0.1 and R=-0.5 tests conducted at the same frequency and at almost the same extreme temperatures of the non-isothermal cycle. It is remarkable that between all the tests the non-isothermal one have the lowest curve slop. Indeed, the loss of the "negative load" crack advance of non-isothermal test is more rapid than that of the R=-0.5/100℃ test since it has higher "negative load" temperature. However the gradual loss of the crack growth rate due to negative loads is the same for the non-isothermal and the R=-0.5/150℃ tests, but the latter has higher "positive load" crack growth rate since it corresponds to higher temperature.

It is worth emphasizing that crack growth rate of the non-isothermal test at ΔK=20 (K_{max}=13.3) corresponding exclusively to the positive load crack growth (at ~90℃) is equal to the da/dN obtained at R=0.1/100℃ for the same K_{max} value, similarly between R=-0.5/150℃ and R=0.1/150℃ tests at K_{max}=13.3, as shown in figure 6.b. Assuming then, that the crack growth rate due to the tension load part of a negative load ratio cycle is equal to the total crack growth rate of a R=0 cycle for the same K_{max}, T and f values permits to write:

$$\left(\frac{da}{dN}\right)^{noniso}_{R<0/K_{max}} = \left(\frac{da}{dN}\right)^{T_{\sigma max}}_{R0/K_{max}} + \left(\frac{da}{dN}\right)^{T_{\sigma min}}_{R<0/K_{max}} - \left(\frac{da}{dN}\right)^{T_{\sigma min}}_{R0/K_{max}} \quad (1)$$

By applying equation (1), the non-isothermal crack growth rate calculation based on the isothermal test results has been done. Figure 6.b shows clearly that the calculated da/dN fits perfectly the non-isothermal test result curve. This verifies that, for cyclic loading, the crack growth rate under non-isothermal negative load ratio can be deduced from the crack growth rates under isothermal positive and negative load ratios conditions.

4 – CRACK GROWTH LAW

The crack growth models based on the energy balance in the continuum thermodynamics framework approach could be good methods to predict the crack advance under non-isothermal condition. Since, it may prevent the use of the stress intensity factor and therefore the use of several parameters that have to be identified and that vary explicitly in accordance with the temperature and other loading specifications. However, such an approach has also some important limitations as it can be applied under constant amplitude loading restrictively. Moreover, the energy balance based crack growth laws require the calculation of the local residual stress fields [8] or the crack opening due to the crack tip plastic zone [9] and to the local plasticity at the eutectic regions. However, our finite element simulation model does not consider the presence of the Si particles in the structure, cause of the local plasticity phenomenon. Therefore, the energy balance approach cannot be used in our case and a method based on a corrected linear elastic fracture mechanics stress intensity factor K_p considering the fatigue, the time dependent, and the negative load effects at non-isothermal condition is introduced:

$$\left(\frac{da}{dN}\right)^{\text{noniso}}_{R<0} = A_1\left(T_{\sigma\max}, f, R\right)\left(\Delta K_p^+\right)^m + A_2\left(R, f\right)\int_0^{t^+} A_3\left(T(t)\right)\left(\delta K_p^+(t)\right)^m .dt + A_4\left(T_{\sigma\min}, f, R\right)\left(\Delta K^-\right)^{m_1\left(T_{\sigma\min}, f, R\right)} \quad (2)$$

Where A_1, A_2, A_3, A_4 and m_1 are the law parameters and the "+" and "-" exponents represent respectively the cycle positive and negative load parts. The stress intensity factor corrected value should account for the cumulative damage induced by the crack tip plasticity, responsible for the history effect. Therefore an iterative model is introduced cumulating the crack tip plasticity, at a crack length $a_{(i)}$, from a cycle *i-j* to the cycle *i*, where *i* is the current cycle and *j* is the number of cycles corresponding to a crack growth equal to the plastic zone size $r_{p(i)}$ calculated at the *i* cycle:

$$\Delta K^+_{p(i)} = K^+_{p(i)}(1-R) \quad (3)$$

Where K_p^+ is calculated as

$$K^+_{p(i)} = \sqrt{\frac{J_{(i)}.E}{1-\nu^2}} \quad (4)$$

J values are determined by summing the elastic contributions represented by the maximum stress intensity factor K^+ to the cumulative plastic term J_p^*:

$$J_{(i)} = \frac{\left(K^+_{(i)}\right)^2\left(1-\nu^2\right)}{E} + J_p^* \quad (5)$$

Where

$$J_{\mathrm{p}}^{*} = \sum_{x=<i-j>}^{i} J_{\mathrm{C}(x)} - \frac{\left(K_{(x)}^{+}\right)^{2}\left(1-\nu^{2}\right)}{E} \tag{6}$$

Where J_{C} is the numerically calculated J value for each cycle. Considering that the crack growth rate remains constant when the crack advances of a length equal to the plastic zone size (from cycle *i-j* to cycle *i*) and that the plastic zone size at a cycle *i* ($r_{p(i)}$) is equal to that at the cycle *i-j* ($r_{p(i-j)}$) yields:

$$j = \frac{r_{\mathrm{p}(i)}}{da \,/\, dN_{(i)}} \tag{7}$$

The $\delta K_{\mathrm{p}}^{+}$ term in equation (2) represent the corrected positive load stress intensity factor for each increment of the cycle ($\delta K_{\mathrm{p}}^{+} = K_{\mathrm{p}(n)}^{+} - K_{\mathrm{p}(n-1)}^{+}$, where *n* is the increment number) and is determined by the same set of equations (3 to 7) used for $\Delta K_{\mathrm{p}}^{+}$.

5 – CONCLUSIONS

Fatigue crack of the A356 alloy free of casting defects is essentially governed by the K_{max} and the material microstructural features (SDAS, Si particles shape and size, etc).
A356 fatigue behavior shows a progressive mixed mechanism crack growth that goes from a total fatigue crack advance at low values of K_{max} through a mixed fatigue/static load cracking to a total crack progression under static load at the end of the Paris regime.
At high temperatures and low frequency, time dependent crack growth constitutes the major part of the crack advance.
Negative parts of loading cycles engender important crack growth rates caused by a local plasticity phenomenon inducing local residual tension stress fields. The compressive load effect on the global crack growth is subjected to a saturation or limitation phenomenon.
For cyclic loading, non-isothermal negative load ratio crack growth rates can be deduced from those obtained under isothermal positive and negative load ratios conditions.
A new non-isothermal crack growth law based on a corrected stress intensity factor K_p accounting for the plasticity history effect is introduced. The law figures all of fatigue, time dependent, and compressive loads effects.

REFERENCES:

[1] Tack AJ, Beevers CJ. The influence of compressive loading on fatigue crack propagation in three aerospace bearing steels. In: 4th International conference on fat. and fat. thresholds, UK: MPCE Ltd; Honolulu, 15–20 July 1990. p. 1179–84.
[2] Pommier S, Prioul C, Bompard P. Influence of a negative R ratio on the creep fatigue behaviour of the N18 nickel base superalloy. Fatigue Fract Eng Mater Struct 1997;20(1):93 107.
[3] Gall K., Yang N., Horstemeyer M., Mcdowell D.L. and Fan J., The debonding and fracture of Si particles during the fatigue of a cast Al–Si alloy. Metall Mater Trans A;30A(12):3079–88, 1999.
[4] Lados D.A., Apelian D., and Major J.F. Fatigue crack growth mechanisms at the microstructure scale in Al–Si–Mg cast alloys: mechanisms in Regions II and III. Metall Mater Trans A;37A(8):2405–18, 2006.
[5] Silva FS. Crack closure inadequacy at negative stress ratios. Int J Fatigue 2004;26:241–52.
[6] Hermann R. Fatigue crack growth in ductile materials under cyclic compressive loading. Fatigue Fract Eng Mater Struct 1994;17(1): 93–103.
[7] Kasaba K, Sano T, Kudo S, Shoji T, Katagiri K, Sato T., Fatigue crack growth under compressive loading. J Nucl Mater 1998;258–263:2059–63.
[8] Wang QG, Apelian D, Lados DA. Fatigue behavior of A356/357 aluminum cast alloys. Part II. Effect of microstructural constituents. J Light Met 2001;1(1):85–97.
[9] Pommier S. Risbet M. Time derivative equations for mode I fatigue crack growth in metals. Int J Fatigue 2005;27:1297–1306.